Numerical Validation of the Shear Compression Specimen. Part I: Quasi-static Large Strain Testing

by A. Dorogoy and D. Rittel

ABSTRACT—The shear compression specimen (SCS), which is used for large strain testing, is thoroughly investigated numerically using three-dimensional elastoplastic finite element simulations. In this first part of the study we address quasi-static loading. A bi-linear material model is assumed. We investigate the effect of geometrical parameters, such as gage height and root radius, on the stress and strain distribution and concentration. The analyses show that the stresses and strains are reasonably uniform on a typical gage mid-section, and their average values reflect accurately the prescribed material model. We derive accurate correlations between the averaged von Mises stress and strain and the applied experimental load and displacement. These relations depend on the specimen geometry and the material properties. Numerical results are compared to experimental data, and an excellent agreement is observed. This study confirms the potential of the SCS for large strain testing of material.

KEY WORDS—Large strain, shear compression specimen, elastic plastic material, finite elements, quasi-static

Introduction

Large shear strains are found in many applications, such as (high-speed) machining, ballistic failure, ductile fracture, and micromechanics of void growth and coalescence. The large strain constitutive behavior of a material has therefore to be determined for modeling and calculation purposes. However, inherent experimental limitations such as necking, barreling or buckling, all affect the various specimens to date, so that large strains are not easily obtainable. Numerous examples can be found in the literature, of original specimen analyses and/or testing procedures used to investigate the large strain plastic properties of materials, such as sheet metal[1] and composites under shear.[2] Other examples can be found in the work of Khan and Wang,[3] who developed a two stage procedure to achieve finite strains in 1100 aluminum, with emphasis on modeling various loading paths. Wang and Lee[4] proposed a numerical modeling procedure to address wrinkling problems in thin sheets. Nouailhas and Cailletaud[5] used crystal plasticity in conjunction with finite element simulations to investigate single-crystal superalloys. Moreover, when shear loading is addressed, the load–displacement curves are readily translated into shear stress–shear strain curves, assuming that shear is the only mode of deformation. However, the use of various specimens, including even the "simplest" torsion cylinder, or more sophisticated shear specimens,[2] may require numerical simulations to assess the validity of certain assumptions, such as homogeneity of the stresses and strains. Numerical simulations are also frequently used to develop various dynamic tests, such as adiabatic shear testing.[6] It also seems that, in most cases, the experimentalist must use several specimen geometries to cover a wide range of strain rates and large strains if possible. Consequently, one would want to use single specimen geometry to cover in a seamless manner the largest possible range of strain rates while allowing for large strains to develop. The shear compression specimen (SCS), suggested by Rittel et al.,[7,8] was specially designed to answer these needs. The specimen, of a very simple geometric shape, consists basically of a cylinder or a parallelepiped with a couple of opposite slots machined at 45° on its faces. As the specimen is axially loaded (either dynamically or statically), the gage (slot) experiences a dominant state of shear. However, as emphasized in all the above-mentioned references, one should not assume a state of pure shear, as preliminary numerical calculations[7] have clearly shown that the state of stress is three-dimensional. Consequently, it was proposed to base the analysis on the von Mises equivalent stress and strain definitions. The validity of the specimen was further established by comparing stress–strain data obtained with the SCS to those obtained from uniaxial (tension/compression) tests.[7–9] However, while the first report[7] suggested simple "universal" approximations for the effective stress and strain as a function of the load and displacement respectively, further work suggested that these approximations should be fine-tuned to the material itself and to the gage geometry.[9] Several fundamental issues have only been addressed in a preliminary manner to date, in the sense that the numerical results were based on a single representative finite element at the center of the gage section, without further averaging of the mechanical fields. Issues, such as the uniformity of the stress and strain throughout the gage, as well as the nature of the stress concentration in the gage fillet and its influence on the determination of the mechanical properties, still remain open. Finally, the central assumption that the same approach (data reduction technique) applies identically to quasi-static and dynamic testing has only been validated experimentally to date.[9] Consequently, a comprehensive numerical study was carried out to assess the advantages and limitations of this new specimen, with emphasis on the above-mentioned issues and keeping in mind simple stress–strain data reduction techniques. Our two-part study

A. Dorogoy is a Postdoctoral Fellow and D. Rittel (SEM Member, meritel@tx.technion.ac.il) is an Associate Professor, Mechanical Engineering Department, Technion—Israel Institute of Technology, 32000, Haifa, Israel.

Original manuscript submitted: July 6, 2004.
Final manuscript received: January 4, 2005.
DOI: 10.1177/0014485105052325

addresses both quasi-static and dynamic loading conditions. This first part concerns quasi-static loading.

The paper is organized in four sections. This first section introduces the subject of this work. The second section presents the investigation of the SCS subjected to quasi-static loading. The results are discussed in the third section, followed by a concluding section.

The second section is divided into seven subsections. The first subsection introduces the SCS geometry and the material properties which were used in this study. The numerical model and data processing technique are detailed in the second subsection. The third subsection presents the numerical results. These results address issues that were not previously addressed, such as (i) the effects of different plastic moduli, gage height, and yield stress on the load–displacement curves, (ii) the evolution and uniformity of the plastic zone, (iii) the influence of the plastic modulus and gage height on the averaged values of stresses and strains in a typical mid-section of the gage, and (iv) the influence of gage root radius. The fourth subsection introduces mathematical approximations of averaged stresses and strains. This subsection describes the relationship between the averaged von Mises stress and strain to the applied load and displacement, respectively. A general approach for the assessment of the plastic modulus is developed in the fifth subsection. Two experimental procedures for the determination of the plastic modulus in a quasi-static test are introduced. These procedures are followed by a reintroduction of a simple stress–strain determination procedure of highly practical relevance to the experimentalist. The dependence of its three coefficients on the plastic modulus and gage width is also detailed. Numerical verification problems are presented in the sixth subsection, followed by a limited experimental validation.

Investigation of the SCS Subjected to Quasi-static Loading

Specimen Geometry and Material Data

The SCS is shown in Fig. 1. As mentioned in the introductory section, this specimen promotes shear deformation in an inclined gage section, and it is aimed at large-strain constitutive testing of materials under both quasi-static and dynamic loading conditions.[7,8] For all the investigated cases, the length, diameter, gage thickness, and root corner radius were chosen to be $L = 20$ mm, $D = 10$ mm, $t = 2.5$ mm, and $R_1 = 0.125$ mm, respectively. Four different slot widths were selected: $w = 0.25$, 0.5, 1.0, and 2.0 mm. The influence of three different root corner radii, $R_1 = 0.125$, 0.25, and 0.4 mm, was also investigated for a gage width of $w = 1.0$ mm. These sets of geometrical parameters cover most of the actual experimental conditions.

The specimen material is assumed to be bi-linear with Young's modulus $E = 210$ GPa, Poisson's ratio $\nu = 0.3$ and yield stress $\sigma_Y = 0.7$ GPa. Three representative hardening moduli were analyzed: $E_p = E/100$, $E_p = E/500$, and $E_p = E/2000$. These values are meant to simulate materials with "high", "average", and "low" hardening characteristics, again to represent a vast class of material behaviors.

Numerical Model

The numerical analysis was carried out using the commercial finite element code ANSYS (Release 7.0, Ansys Inc.). Due to the symmetry of the problem, only one half of the specimen is modeled, as can be seen in Fig. 2. A typical mesh, which consist of 20335 elements of ANSYS type SOLID187 (3-D 10-Node Tetrahedral Structural Solid), is shown in Fig. 2.

Traction-free boundary conditions were applied on all surfaces, except for surfaces A9, A11, and A13, as shown in

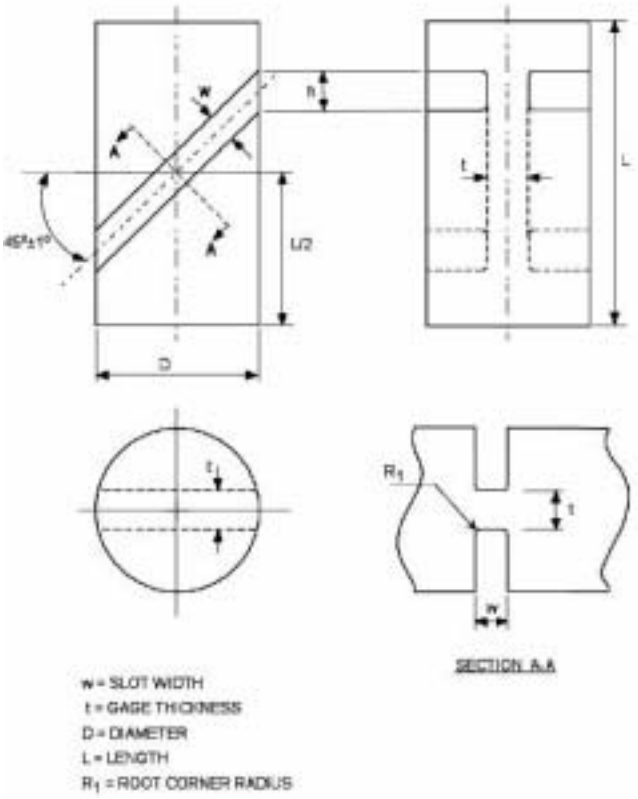

Fig. 1—The shear compression specimen

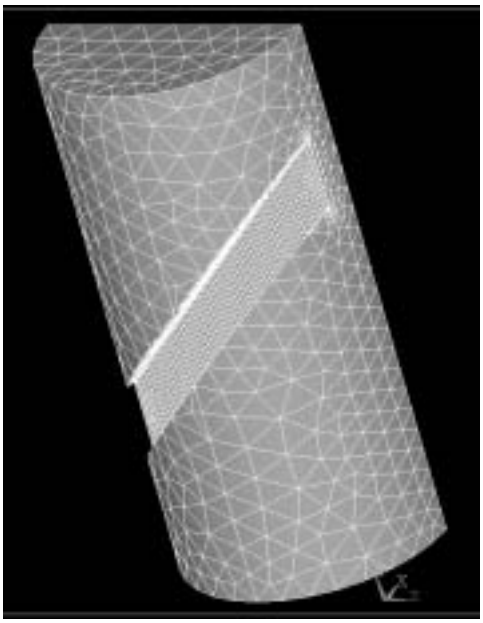

Fig. 2—The meshed half SCS

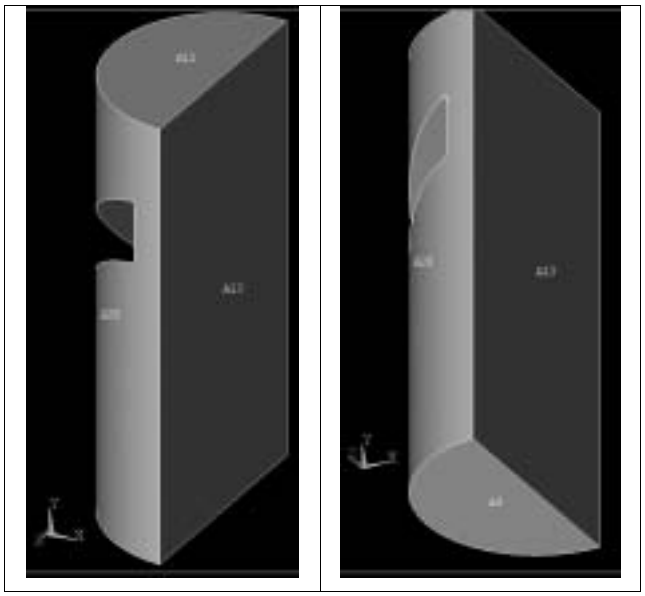

Fig. 3—Constrained surfaces

Fig. 3. Symmetry conditions were enforced on surface A13, while surface A9 was constrained from vertical (y) motion and totally constrained at an arbitrary point. A displacement boundary condition of $d = –1.75$ mm along the y-direction was applied on surface A11.

The non-linear equilibrium equations are solved implicitly and incrementally (see ANSYS, Release 7.0, Theoretical Manual, Ansys Inc.). The non-linearity includes material and geometrical effects, namely plasticity and large strains. At each load step i ($1 < i < N$) the applied displacement d_i is known, and the resulting pressure force P_i at the upper surface (A11) is calculated by integrating the normal stresses σ_{yy} over the surface A11.

Averaged values of the equivalent von Mises stress ($\hat{\sigma}_{eqv}$), hydrostatic stress ($\hat{\sigma}_{hyd}$), and the equivalent total strain ($\hat{\varepsilon}_{eqv}$) on the inclined mid-section of the gage are calculated at each load step. The inclined mid-section of the gage is shown in Fig. 4, where the upper half of the specimen has been removed. The averaged values are calculated by integrating the stresses on the mid-section and dividing them by the area of the plane, according to

$$\hat{\sigma}_{eqv} = \frac{1}{A}\int_A \sigma_{eqv}\,\mathrm{d}A \tag{1}$$

$$\hat{\varepsilon}_{eqv} = \frac{1}{A}\int_A \varepsilon_{eqv}\,\mathrm{d}A \tag{2}$$

$$\hat{\sigma}_{hyd} = \frac{1}{A}\int_A \sigma_{hyd}\,\mathrm{d}A. \tag{3}$$

Results

LOAD-DISPLACEMENT

During an experiment, the enforced displacement (d) on the upper surface (A11 in Fig. 3) and the resulting (negative)

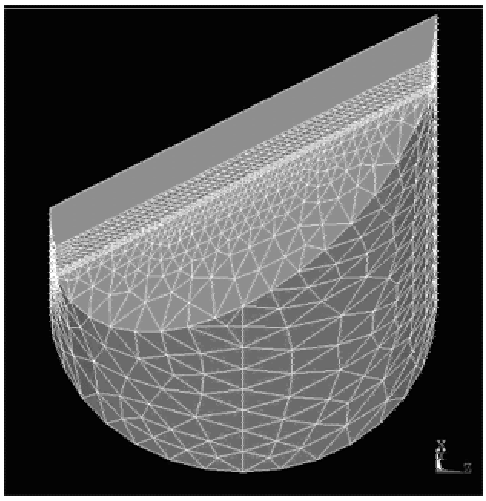

Fig. 4—The inclined mid-section of the gage where the averaged $\hat{\sigma}_{eqv}$, $\hat{\sigma}_{hyd}$, and $\hat{\varepsilon}_{eqv}$ are calculated

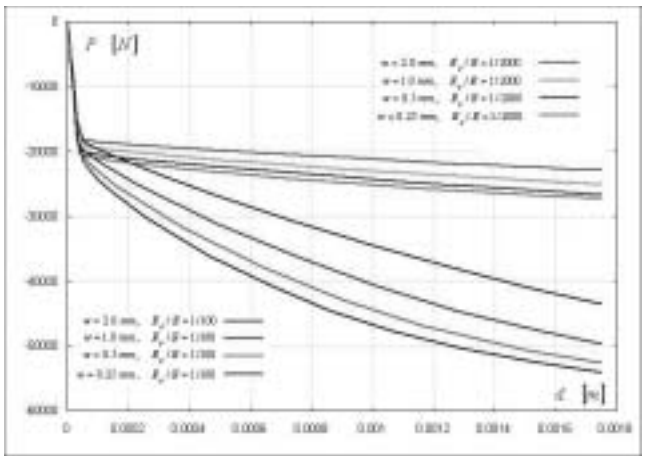

Fig. 5—Resultant load–displacement curves for SCS specimens

load (P) are measured. The resultant $P - d$ curves for four different gage heights, $w = 0.25$, 0.5, 1.0, and 2.0 mm, are plotted in Fig. 5. Two hardening moduli were considered: $E_p = E/2000$ ("soft") and $E_p = E/100$ ("hard"). All the curves coincide until the load reaches –18,000 N (approximately), as a macroscopic indication for the end of the elastic region. This figure shows that for a decreasing gage height, a higher compressive load is needed to enforce the same displacement. The bi-linear nature of the constitutive equations is reflected on the $P - d$ curves for the "soft" material while the "hard" material exhibit a non-linear behavior, as noticeable from the curvature of the $P - d$ curves.

The specimen with $w = 2$ mm was analyzed one more time, assuming now a yield stress $\sigma_Y = 1200$ MPa instead of $\sigma_Y = 700$ MPa. The resulting $P - d$ plots are shown in Fig. 6. The analyses demonstrate that the yield load is proportional to the assumed yield stress, as expected.

STRESS AND STRAIN DISTRIBUTION IN THE GAGE

In this section we first describe the stress and strain distribution in the whole specimen, followed by their distribution

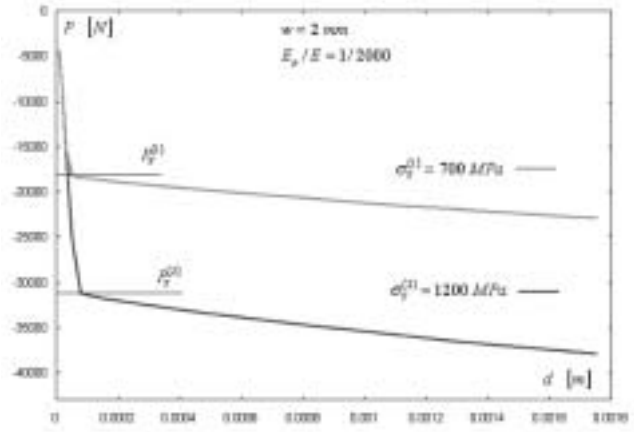

Fig. 6—Resultant load–displacement plots for $\sigma_Y^{(1)}$ = 700 MPa and $\sigma_Y^{(2)}$ = 1200 MPa

on a representative mid-section of the gage. A contour plot of the von Mises equivalent stress on surface A13 of Fig. 3 is plotted in Fig. 7 for two different hardening materials. The plot represents a specimen of $w = 2$ mm with prescribed displacement of $d = 1.75$ mm.

The minimum value for the contour plot was chosen to be $\sigma_{eqv} = \sigma_Y = 700$ MPa. This value was chosen in order to emphasize the regions which have undergone plastic deformation. The plastic zones corresponding to $E_p = E/2000$ and $E_p = E/100$ are shown in Figs. 7(a) and (b), respectively. The plastic zone for $E_p = E/2000$ is mostly confined to the gage, while for $E_p = E/100$ the plastic zone spreads into the whole specimen. This fact might explain the nonlinear behavior of the $P - d$ curves for $E_p = E/100$ in Fig. 5.

An important point is that of the uniformity of stress and strain on a typical mid-section of the gage. As in any experimental specimen geometry, one cannot expect these quantities to be strictly uniform, and this point is quite important to assess the quality of experimental results. We selected a specimen of 2 mm gage height, subjected to a displacement of 1.75 mm, with $E_p = E/100$. This high plastic modulus value was selected to represent the "worst" case in which plasticity spreads out of the gage. The distribution of σ_{eqv}, ε_{eqv}, and σ_{hyd} on the mid-section is presented in Fig. 8.

Averaging σ_{eqv} by means of eq (1) yields $\hat{\sigma}_{eqv} = 1.501$ GPa. Figure 8(a) reveals that σ_{eqv} is not strictly uniform on the mid-section, but is in the range $0.87 \leq \sigma_{eqv}/\hat{\sigma}_{eqv} \leq 1.1$. Most of the area of the section experiences a stress level of $0.97 \leq \sigma_{eqv}/\hat{\sigma}_{eqv} \leq 1.05$, which is confined within 5% of the average value. Yet, the present results indicate a high degree of homogeneity of the mechanical fields, which is quite appropriate to engineering testing of mechanical behavior of materials.

Averaging ε_{eqv} by means of eq (2) yields $\hat{\varepsilon}_{eqv} = 0.386$. Figure 8(b) reveals that ε_{eqv} also is not strictly uniform on the mid-section, but is on the range $0.73 \leq \varepsilon_{eqv}/\hat{\varepsilon}_{eqv} \leq 1.14$. Most of the area of the section experiences a strain level of $0.88 \leq \varepsilon_{eqv}/\hat{\varepsilon}_{eqv} \leq 1.06$, which is confined within 12% of the average value.

Averaging σ_{hyd} by means of eq (3) yields $\hat{\sigma}_{hyd} = -0.378$ GPa. Figure 8(c) reveals that the hydrostatic stress

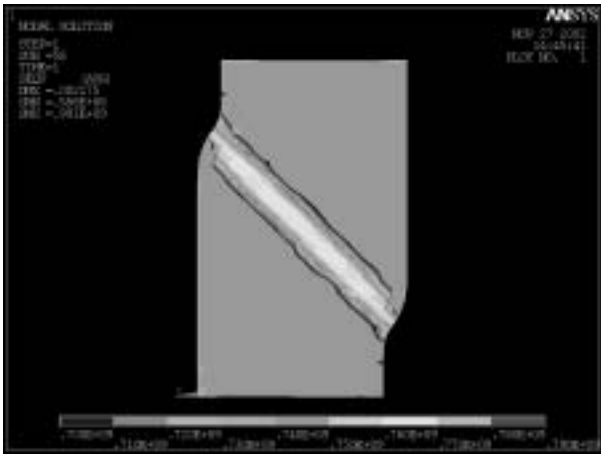

7a

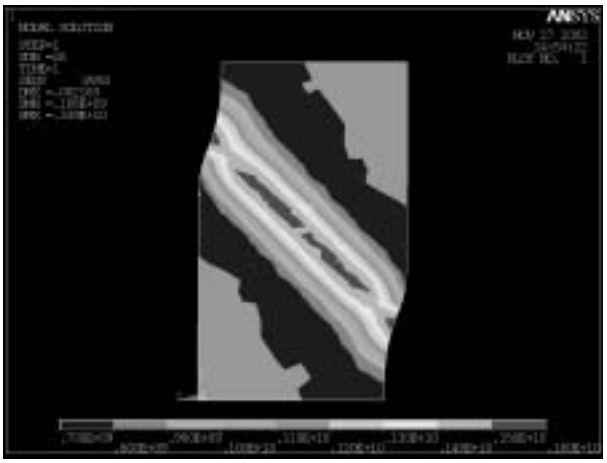

7b

Fig. 7—Plastic zones for a specimen of w = 2 mm with enforced displacement of d = 1.75 mm: (a) plastic zones for $E_p = E$ / 2000; (b) plastic zones for $E_p = E$ / 100

too, σ_{hyd}, is not uniform on the mid-section but is in the range $0.53 \leq \sigma_{hyd} / \hat{\sigma}_{hyd} \leq 1.85$. Most of the area of the section experiences a stress level of $0.82 \leq \sigma_{hyd} / \hat{\sigma}_{hyd} \leq 1.11$, which is confined within 18% of the average value.

Averaged Values of Stresses and Strains on the Mid-section of the Gage

Another important point is that of the relationship between the average values on the specimen mid-section and the prescribed constitutive law. While one would expect them to be automatically identical, the point must be verified. Figure 9 shows the average stress–strain relation for two different hardening materials, $E_p = E/100,\ E/2000$, and four different gage heights, $w = 0.25$, 0.5, 1.0, and 2.0 mm. Figure 9 clearly indicates that the prescribed constitutive relations are recovered by all four gages for the two hardening moduli. Additional information is gained by estimating the relative error that arises in the estimation of the plastic modulus. Table 1 summarizes results of linear regressions made on the results of Fig. 9. The result of the linear regression E_p^* is compared to the real hardening modulus E_p. The maximum difference from the real modulus was found to be 33 MPa, which is less than 1.6% error for $E_p = E/100$. The relative errors for the soft material with $E_p = E/2000$ are greater and reach 13% because of the small value of the hardening modulus. These

TABLE 1—COMPARISON BETWEEN COMPUTED HARDENING MODULUS BY LINEAR REGRESSION AND THE REAL HARDENING MODULUS

w (mm) Gage Height	E_p (10^9 Pa)	E_p^* (10^9 Pa) Linear Regression	$E_p - E_p^*$ (10^9 Pa) Difference	$(E_p - E_p^*) / E_p$ Difference (%)
0.25	2.1	2.102	–0.002	–0.1
0.50	2.1	2.133	–0.033	–1.6
1.0	2.1	2.127	–0.027	–1.3
2.0	2.1	2.120	–0.020	–1.0
0.25	0.105	0.103	0.002	1.9
0.50	0.105	0.100	0.006	5.3
1.0	0.105	0.091	0.014	13.2
2.0	0.105	0.102	0.003	2.9

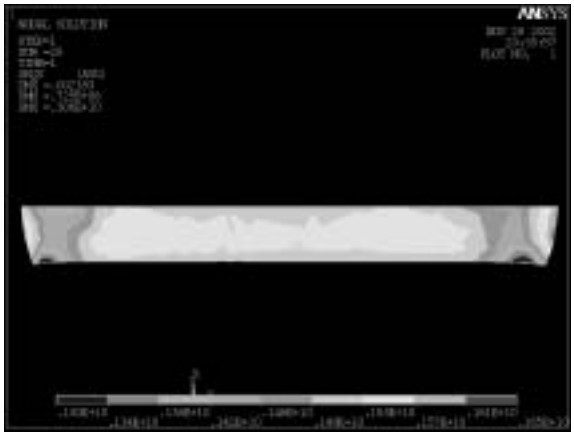

8a

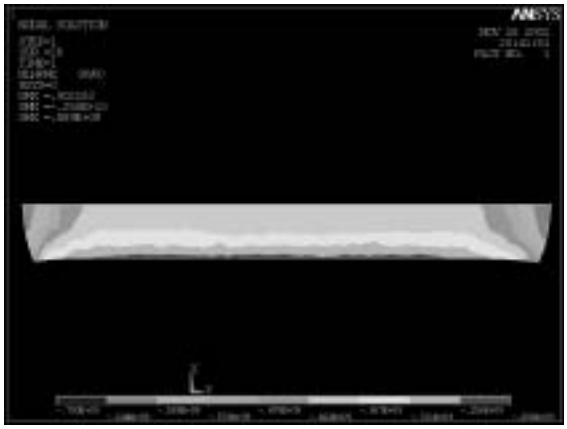

8b

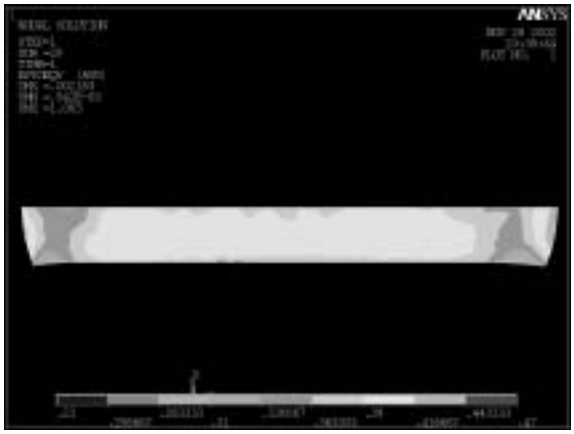

8c

Fig. 8—Typical variation of σ_{eqv}, ε_{eqv}, and σ_{hyd} on the section shown in Fig. 4 for a 2 mm height gage subjected to a displacement of 1.75 mm with E_p = E / 100: (a) contour map of σ_{eqv}; (b) contour map of ε_{eqv}; (c) contour map of σ_{hyd}

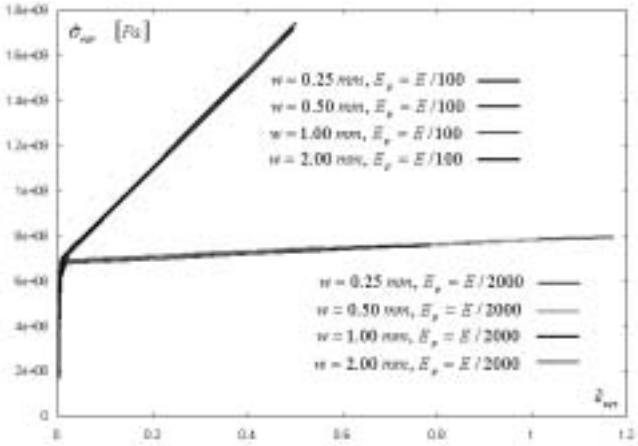

Fig. 9—$\hat{\sigma}_{eqv}$ versus $\hat{\varepsilon}_{eqv}$ for specimens of gage heights 0.25, 0.5, 1, and 2 mm made of two different materials which differ in their hardening modulus: E/100 and E/2000. Note that the prescribed constitutive law is exactly represented by these average values

results show that the specimen can be reliably used and data processed for experimental testing of materials.

The averaged hydrostatic stress $\hat{\sigma}_{hyd}$ versus $\hat{\varepsilon}_{eqv}$ is plotted in Fig. 10 for the above-mentioned cases. The figure reveals that the hydrostatic stresses are all negative and increase (in absolute value) as the gage height decreases. The "hard" material reaches higher hydrostatic stresses, which change more steeply with increasing strain $\hat{\varepsilon}_{eqv}$. It can also be observed in Figs. 9 and 10 that the smaller the gage height, the greater the averaged total strain.

The variation of $\left|\hat{\sigma}_{hyd}/\hat{\sigma}_{eqv}\right|$ is plotted in Fig. 11. As before, four different gage heights are examined: $w = 0.25$, 0.5, 1.0, and 2 mm. Figure 11(a) is for hardening modulus of $E_p = E/100$ and Fig. 11(b) is for hardening material of $E_p = E/2000$. Figure 11 reveals that for $E_p = E/100$ and all the gage heights examined, this ratio is $0.52 < \left|\hat{\sigma}_{hyd}/\hat{\sigma}_{eqv}\right| < 0.25$. For $E_p = E/2000$ and all the gage heights examined, this ratio becomes $0.54 < \left|\hat{\sigma}_{hyd}/\hat{\sigma}_{eqv}\right| < 0.20$. The ratio of $\left|\hat{\sigma}_{hyd}/\hat{\sigma}_{eqv}\right|$ does not change significantly during the loading of a specimen; for example, for the specific gage height $w = 0.5$ mm and $E_p = E/2000$ this ratio is $0.39 < \left|\hat{\sigma}_{hyd}/\hat{\sigma}_{eqv}\right| < 0.48$. All the above results indicate a variable state of triaxiality, as compared to a uniaxial type of specimen. They also show that the hydrostatic to

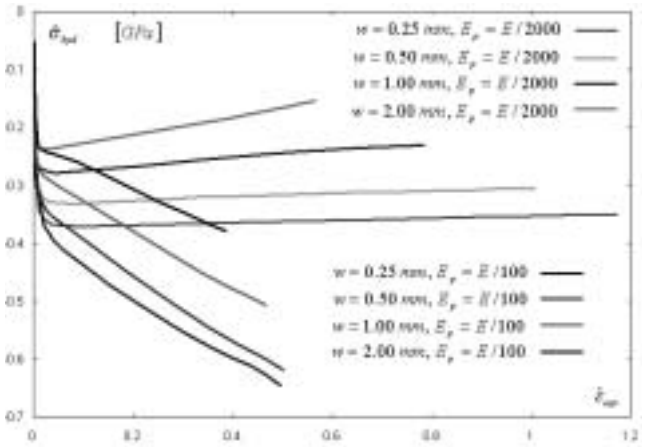

Fig. 10—Averaged hydrostatic stresses versus the averaged equivalent total strain on the mid-section of Fig. 4

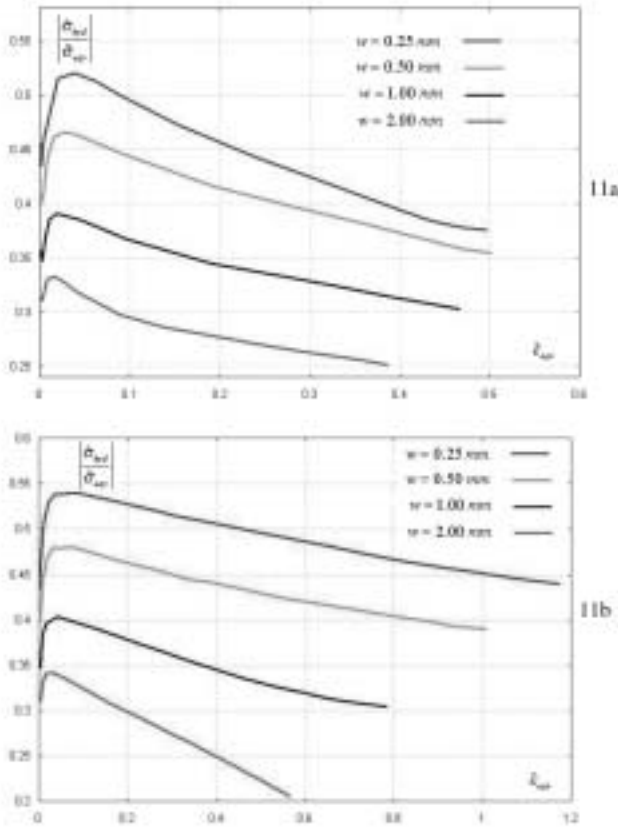

11a

11b

Fig. 11—The variation of the ratio between $\hat{\sigma}_{hyd}$ to $\hat{\sigma}_{eqv}$ on the mid-section versus $\hat{\varepsilon}_{eqv}$: (a) E_p = E / 100; (b) E_p = E / 2000

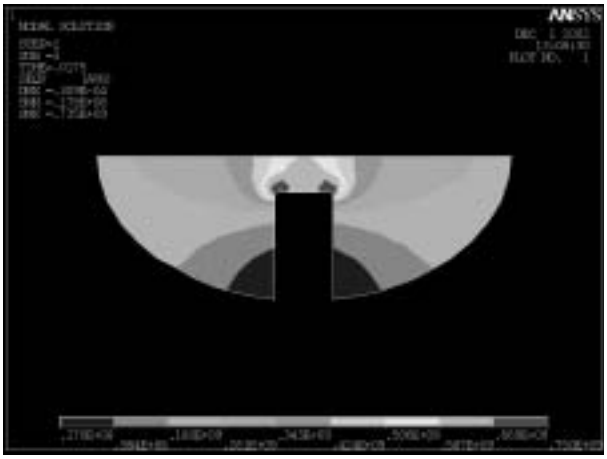

12a

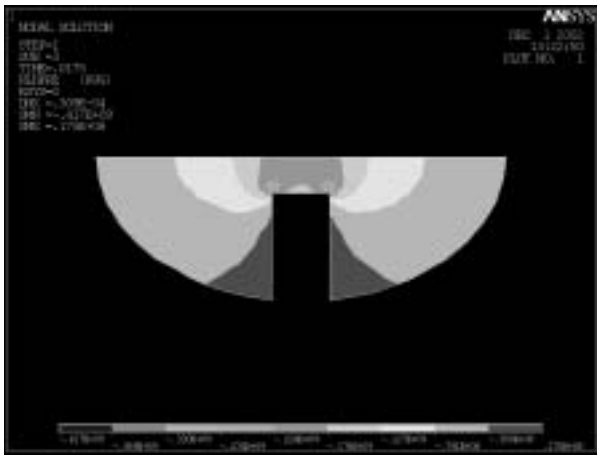

12b

Fig. 12—Contour maps of $\hat{\sigma}_{eqv}$ and $\hat{\sigma}_{hyd}$ on the cross-section A–A of Fig. 1: (a) $\hat{\sigma}_{eqv}$; (b) $\hat{\sigma}_{hyd}$

equivalent stress ratio is relatively insensitive to the constitutive behavior of the material.

Effect of Gage Root Radius

As with any other specimen, the influence of local stress concentrations is assessed to estimate the reliability of the future experimental results obtained using this specimen. For this reason, three specimens of $w = 2$ mm and hardening modulus of $E_p = E/500$, which differ by their gage root radius, were analyzed (all other material and geometrical properties remained identical). The selected root radii are $R_1 =$ 0.125, 0.2, 5, and 0.4 mm. The distributions of the stresses $\hat{\sigma}_{eqv}$ and $\hat{\sigma}_{hyd}$ on the cross-section shown in Fig. 4 are plotted as contour maps in Fig. 12. The maps were generated for the smallest root radius of $R_1 = 0.125$ mm and for applied displacement of 3×10^{-5} m. At this displacement level, the material adjacent to the root radius just starts to yield. It can be noticed that the effect of the corner radius is mostly confined to the corner.

The effect of the selected root radii on the $\hat{\sigma}_{eqv} - \hat{\varepsilon}_{eqv}$ graph is shown in Fig. 13. It can be observed that the three corner point radiuses yield the same characteristic mechanical behavior. Decreasing the root radius causes a slight increase in $\hat{\sigma}_{eqv}$ and $\hat{\varepsilon}_{eqv}$. The presence of a sharp corner does not affect the ability to reconstruct the characteristic behavior of the material from the $\hat{\sigma}_{eqv} - \hat{\varepsilon}_{eqv}$ graph.

The effect of the selected root radii on the $\hat{\sigma}_{hyd} - \hat{\varepsilon}_{eqv}$ graph is shown in Fig. 14. It can be observed that decreasing the root radius causes a slight decrease in $|\hat{\sigma}_{hyd}|$.

These results indicate that when $0.125 < R_1 < 0.4$ mm, stress concentration near the root radius has a negligible influence on the calculated averaged mechanical properties.

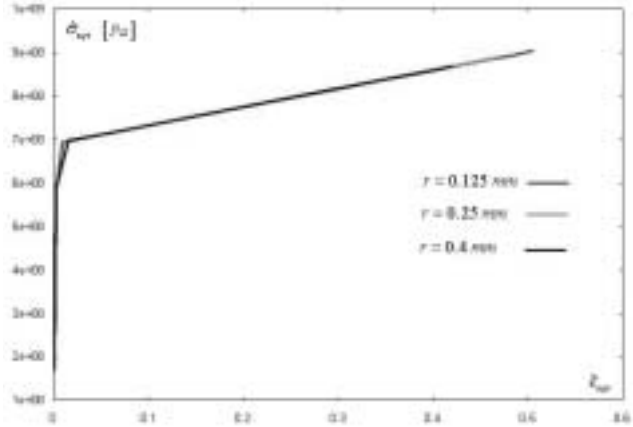

Fig. 13—$\hat{\sigma}_{eqv} - \hat{\varepsilon}_{eqv}$ graph of a w = 2 mm gage with hardening modulus of E_p = E / 500 made with three different corner point radii: R_1 = 0.125, 0.25, and 0.4 mm

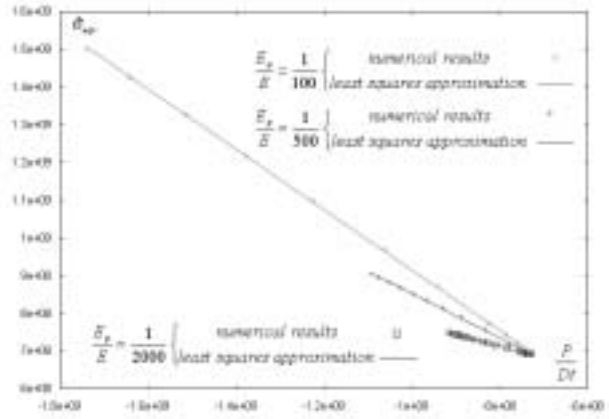

Fig. 15—Numerical results of $\hat{\sigma}_{eqv}$ versus P / Dt and their least-squares polynomial approximation

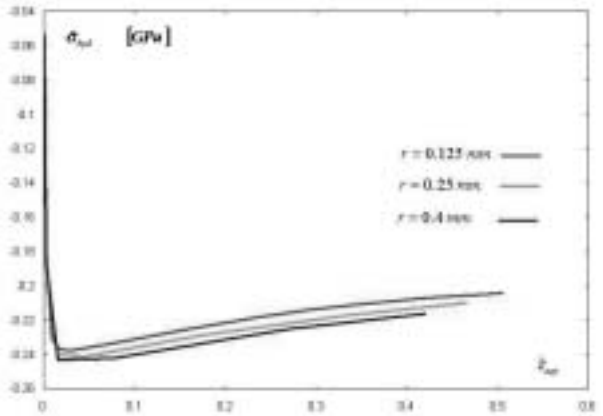

Fig. 14—$\hat{\sigma}_{hyd} - \hat{\varepsilon}_{eqv}$ graph of a w = 2 mm gage with hardening modulus of E_p = E / 500 made with three different corner point radii: R_1 = 0.125, 0.25, and 0.4 mm

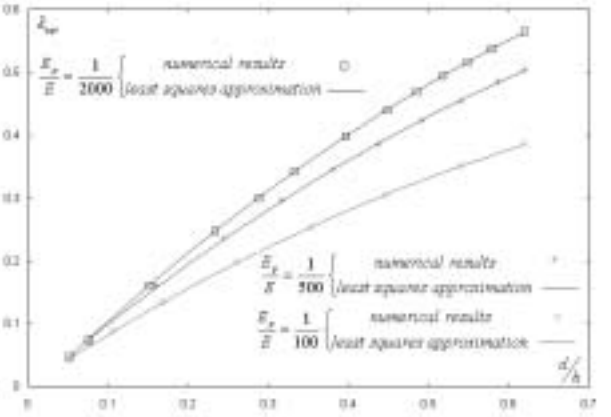

Fig. 16—Numerical results of $\hat{\varepsilon}_{eqv}$ versus d / h and their least-squares polynomial approximation

Approximation of $\hat{\sigma}_{eqv} - \hat{\varepsilon}_{eqv}$ Curve from P–d Data

In this section, we present correlations between $\hat{\sigma}_{eqv}$ and $\hat{\varepsilon}_{eqv}$ and the applied load P and displacement d, respectively. For each kind of specimen (the difference is only the gage height) three numerical analyses are performed for three different ratios of E_p/E . For every ratio, $\hat{\sigma}_{eqv}$ is approximated by a first-order polynomial function of the applied force

$$\hat{\sigma}_{eqv} \cong f_1(P) = c_1 \sigma_Y + c_2 \frac{P}{D\,t} \tag{4}$$

Likewise, $\hat{\varepsilon}_{eqv}$ is approximated by a second-order polynomial of the form

$$\hat{\varepsilon}_{eqv} \cong f_2(d) = c_3 + c_4 \left(\frac{d}{h}\right) + c_5 \left(\frac{d}{h}\right)^2 \tag{5}$$

where $h = \sqrt{2}w$ is the horizontal height of the gage, t is its thickness, and D is the diameter of the specimen. The coefficients $c_i^{(j)}$, $i = 1 \cdots 5$, $j = 1 \cdots 3$, where the superscript $^{(j)}$, $j = 1 \cdots 3$ corresponds to a ratio E_p/E are calculated from the numerical results by using least-squares approximations with the aid of the IMSL Fortran Library, Version 3.0 (Visual Numerics, Inc.). To make eqs (4) and (5) suitable for any ratio of E_p/E the coefficients are approximated by

$$c_i = a_{ij} x_j \tag{6}$$

where

$$x_j = \begin{Bmatrix} 1 \\ \ln(E_P/E) \\ \ln^2(E_P/E) \end{Bmatrix} \tag{7}$$

The coefficients a_{ij} are calculated by solving i systems of j equations. Equations (4)–(6) can be used to approximate the stress–strain curve for any ratio of E_p/E. Verification problems are presented in the following section.

A demonstration of the approximations (4)–(6) is seen in Figs. 15 and 16. For this demonstration, the numerical results of a specimen of $w = 2$ mm with three different plastic moduli ($E_p = E/2000$, $E_p = E/500$, and $E_p = E/100$) are used. In these figures the numerical results are shown as points, and the numerical approximations, eqs (4) and (5), are shown as solid lines. It can be observed that a very good approximation

TABLE 2—COEFFICIENTS OF LEAST-SQUARES APPROXIMATION FOR A SPECIMEN WITH w = 2.0 mm. NOTE THAT c_1 IS DIVIDED BY THE ASSUMED YIELD STRESS OF 700 MPa

E_P / E	c_1 / 700 × 10^6	c_2	c_3	c_4	c_5
1 / 2000	0.6842	–0.2835	–0.0139	1.1895	–0.3575
1 / 500	0.3527	–0.5982	–0.0109	1.1216	–0.4186
1 / 100	0.1037	–0.8329	–0.0029	0.8806	–0.4136

is achieved. Table 2 summarizes the coefficients $c_i^{(j)}$ for the specimen of $w = 2.0$ mm.

Processing of Results

A First Method for the Determination of the Plastic Modulus E_p (Method 1)

The procedure to determine the plastic modulus E_p for large strains from experimental $P - d$ data is as follows.

1. Conduct an experiment with the SCS specimen and obtain the $P - d$ data.
2. Perform numerical analyses of the SCS specimen with three different ratios of E_p/E.
3. From the results of step 2, calculate the coefficients a_{ij} using eqs (3)–(7).
4. Guess an initial value for E_p/E.
5. Calculate $c_i,\ i = 1 \cdots 5$ of eq (6).
6. Use eqs (4) and (5) with the coefficients obtained in step 5 together with the experimental $P - d$ data to obtain the $\hat{\varepsilon}_{eqv} - \hat{\sigma}_{eqv}$ graph.
7. Calculate the slope E_p^* from the $\hat{\varepsilon}_{eqv} - \hat{\sigma}_{eqv}$ graph.
8. Conduct a convergence test: if E_p^* is not equal to the assumed E_p in step 4, then guess another value for E_p/E and go to step 5; if E_p^* is equal to the assumed E_p in step 4, then terminate.

The procedure described in steps 1–8 is incorporated into a minimization procedure of the norm $\left|E_p^* - E_P\right|$.

A Second Method for the Determination of the Plastic Modulus E_p (Method 2)

For each specimen geometry, three different $P - d$ graphs are plotted. The three graphs correspond, as mentioned, to the three different ratios of E_p/E. Each graph can be approximated in the range $d_{min} < d < d_{max}$ by a straight line. The values of d_{min} and d_{max} can be chosen arbitrarily as long as they are greater than d_Y, which is the value of the applied displacement that causes the gage of the specimen to deform plastically, from a macroscopic point of view. The slope of a segment of the $P - d$ graph in the range $d_{min} < d < d_{max}$ is calculated by using least-squares approximation with the aid of the IMSL Fortran Library, Version 3.0 (Visual Numerics, Inc.). The plastic modulus as a function of the slope is approximated by a second-order polynomial

$$E_p(s) = d_0 + d_1\, s + d_2\, s^2 \tag{8}$$

The coefficients $d_i,\ i = 0 \ldots 2$ are calculated by solving the system of equations

$$E_P^{(k)} = d_0 + d_1\, s^{(k)} + d_2\, s^{2(k)}, k = 1 \cdots 3. \tag{9}$$

The procedure to determine the plastic modulus E_p for large strains is thus as follows.

1. Perform an experiment with the SCS specimen and obtain the $P - d$ data.
2. Perform three numerical analyses of the SCS specimen with three different ratios of E_p/E.
3. Plot the three different $P-d$ numerical graphs of step 2 with the experimental $P - d$ graph obtained in step 1.
4. Select the values d_{min} and d_{max}.
5. Calculate the three numerical slopes $s^{(k)},\ k = 1 \cdots 3$ in the range $d_{min} < d < d_{max}$.
6. Calculate the coefficients $d_i,\ i = 0 \ldots 2$ according to eq (9).
7. Calculate the slope s^* in the range $d_{min} < d < d_{max}$ from the experimental $P - d$ graph.
8. Obtain an approximation for E_p^* by substituting s^* in eq (8).

The procedure described in steps 1–8 is incorporated into a computer code which finds automatically the value of E_p^*.

A Simple Method to Determine the Stress–strain Relationship

The stress–strain curve determination was presented originally as a simple expression[7] of three coefficients, k_i (i= 1–3), as follows:

$$\hat{\sigma}_{eqv} = k_1 \left(1 - k_2 \hat{\varepsilon}_{eqv}\right) \frac{P}{D\,t} \tag{10}$$

$$\hat{\varepsilon}_{eqv} = k_3 \frac{d}{h} \tag{11}$$

One would naturally like to develop similar relations that are quite easy to use for the practitioner. Therefore, once E_p^* has been determined using either approach described earlier, its value is substituted into eq (6) to calculate $c_i,\ i = 1 \ldots 5$. The experimental load–displacement data along with eqs (4) and (5) are used to plot the desired stress–strain curve. The curve is fitted with the aid of least-squares to determine the three coefficients k_1, k_2, and k_3. These coefficients, once determined for a given material and gage geometry, will be used to process all the subsequent experimental data.

The Dependence of the k_i Coefficients on Material Properties and Gage Geometry

Specimens with two different gage heights were considered: $w = 1$ and 2 mm. The material properties used in all analyses were $E = 73.8$ MPa, $\nu = 0.33$, and $\sigma_Y = 400$ MPa. A bi-linear material model was assumed. Three different plastic modulus were analyzed for each gage height: $E/E_p = 100$, 500 and 2500. The k_1, k_2, and k_3 coefficients were calculated with the aid of least-squares for each case, as shown in Table 3. From Table 3 it can be concluded that the coefficient k_1 depends on the gage height and almost not on the material properties. On the other hand, k_2 and k_3 are dependent on both the gage height and material properties.

Verification Problems

In order to validate the two data reduction methods and the accuracy of eqs (4) and (5) for E_p/E other than those investigated, two additional cases were solved numerically. The first case involves a specimen with $w = 2$ mm and $E_p/E = 1/300$. The second case involves a specimen with $w = 0.25$ mm and $E_p/E = 1/800$. The obtained numerical (P, d) data served as the "experimental measured results" input for the two processing methods.

For the first case, applying method 1 in the range $0.1 \leq d \leq 1$ mm yields $E_p^*/E = 1/311$. Applying method 2 to the same d range yields $E_p^*/E = 1/300$. The coefficients c_i, $i = 1 \ldots 5$, are obtained by substitution of the average value $\hat{E}_p^*/E = 1/306$ into eq (6). Equations (4) and (5) for the first case become

$$\hat{\sigma}_{eqv} = 0.2837 \times 700 \times 10^6 - 0.6850\frac{P}{Dt} \qquad (12)$$

$$\hat{\varepsilon}_{eqv} = -0.0090 + 1.0663\left(\frac{d}{h}\right) - 0.4258\left(\frac{d}{h}\right)^2. \qquad (13)$$

For the second case, applying method 1 to the range $0.2 \leq d \leq 0.8$ mm yields $E_p^*/E = 1/828$. Applying method 2 to the same d range yields $E_p^*/E = 1/807$. The coefficients c_i, $i = 1 \ldots 5$, are obtained by substitution of the average value $E_p^*/E = 1/817$ into eq (6). Equations (4) and (5) for the second case become

$$\hat{\sigma}_{eqv} = 0.3042 \times 700 \times 10^6 - 0.5911\frac{P}{Dt} \qquad (14)$$

$$\hat{\varepsilon}_{eqv} = -0.01 + 0.3033\left(\frac{d}{h}\right) - 0.0191\left(\frac{d}{h}\right)^2. \qquad (15)$$

From eq (4) it is clear that when $\hat{\sigma}_{eqv} = \sigma_Y$, $P = P_Y$. For this reason in eqs (12) and (14) the coefficient c_1 is slightly modified to

$$c_1^* = 1 - \frac{c_2}{\sigma_Y}\frac{P_Y}{D\,t} \qquad (16)$$

Pairs of data (P, d) which were calculated by the numerical analyses were substituted into eqs (12)–(15) and the resulting curves of $\hat{\varepsilon}_{eqv} - \hat{\sigma}_{eqv}$ are plotted in Fig. 17. The "real" bi-linear $\hat{\varepsilon}_{eqv} - \hat{\sigma}_{eqv}$ curves used in the numerical analyses are compared to the approximation by eqs (12)–(15). Since there is a very good agreement in Fig. 17 for the two cases corresponding to the two extreme gage heights, it can be concluded that the processing methods as well as the approximations are suitable for assessing the constitutive relations, noting that the higher gage yields more accurate results.

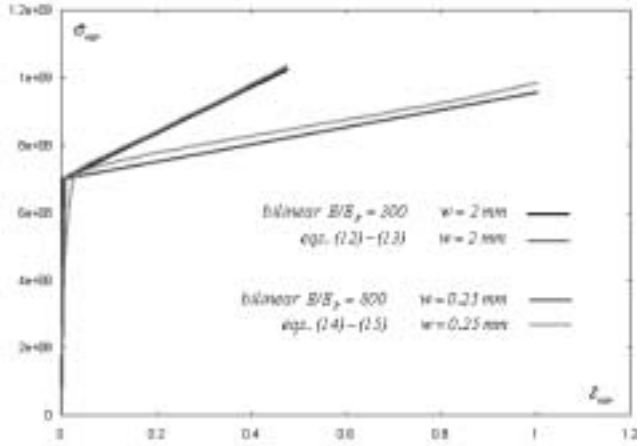

Fig. 17—A comparison between numerical analysis and approximations of the $\hat{\sigma}_{eqv} - \hat{\varepsilon}_{eqv}$ curve

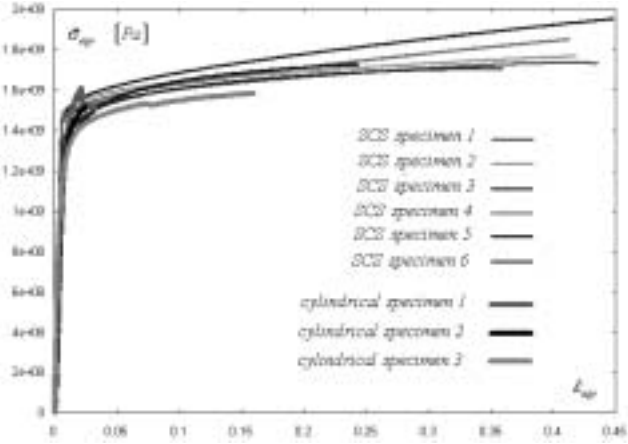

Fig. 18—$\hat{\sigma}_{eqv} - \hat{\varepsilon}_{eqv}$ curves of tungsten alloy obtained by using five SCS specimens and three cylindrical specimens

Experimental Results

SCS specimens made of tungsten heavy alloy were tested for obtaining their characteristic $\hat{\varepsilon}_{eqv} - \hat{\sigma}_{eqv}$ behavior. The results were processed as described in the previous sections. Two parallelepiped SCS specimens with the three different gage widths (0.3, 1, and 2.5 mm) were tested. The specimens were typically 20 mm high, 9.5 mm wide, and 6.5 mm thick. The gage thickness was 2.5 mm. The calculated k_i, $i = 1 \ldots 3$ for each gage width are summarized in Table 4. The SCS results are compared to results obtained by compressing cylinders. The latter are limited to small strains because of barreling, and three typical results are plotted in Fig. 18. For this material, $E/E_p \approx 600$. A good agreement is observed for the two specimen geometries in the comparable range of small strains. It can also be noted that, to a first approximation,

TABLE 3—TYPICAL DEPENDENCE OF THE COEFFICIENTS k_1, k_2, AND k_3 ON THE SPECIMEN'S GAGE HEIGHT AND PLASTIC MODULUS

w (mm)	E / E_p	k_1	k_2	k_3
1	100	0.856	0.056	0.501
	500	0.851	0.142	0.649
	2500	0.848	0.174	0.691
2	100	0.928	0.212	0.739
	500	0.924	0.221	0.915
	2500	0.922	0.231	0.988

TABLE 4—THE CALCULATED COEFFICIENTS k_1, k_2, AND k_3 FOR ANALYZING TUNGSTEN HEAVY ALLOY

w (mm)	k_1	k_2	k_3
0.3	0.861	0.152	0.213
1.0	0.927	0.219	0.628
2.5	0.955	0.276	0.931

this material behaves in a bi-linear fashion. Consequently, the results are believed to be reliable at larger strains for the SCS.

Discussion

The SCS has been modeled and thoroughly analyzed using the finite element method. Several previously unaddressed issues have been investigated and reported: the influence of specimen geometry and material parameters. In addition, a simple data reduction technique has been developed and validated (eqs (10) and (11)). The main points of this study will now be discussed and summarized. The numerical calculations assume a bi-linear elastic–plastic material. While such a behavior is observed in some materials, the more general constitutive response is of the parabolic type. Consequently, the present assumption is an approximation which should be carefully checked for each specific type of material. However, it is felt that as a first approximation, it is satisfactory, keeping in mind that a parametric study of the present time would be difficult to achieve for a parabolic material.

The analyses reveal that the averaged $\hat{\varepsilon}_{eqv} - \hat{\sigma}_{eqv}$ on the mid-section reproduces the constitutive bi-linear equation of the material. This result is not influenced by the yield stresses or specimen geometry (gage height, root radius). This result is backed by the observation that the stress and strain distribution in the gage section of the specimen is reasonably homogeneous. Previous work[7] had not addressed this important issue.

Stress concentration in the gage fillet has been examined in detail for three root radii that are representative of most specimens. Calculations were carried out for quasi-static loading only, but one can reasonably assume that the main findings apply to the dynamic case as well. The results indeed show stress concentration, as expected; however, it does not affect significantly the determination of the stress–strain relationship. One should nevertheless keep in mind that specific issues related to stress concentration may indeed be affected. As an example, shear localization (such as adiabatic shear banding), may indeed be triggered by the local mild stress concentration observed. However, this point is beyond the scope of the present work, as it essentially requires additional experimental and numerical work.

The simple relationship originally proposed by Rittel et al.,[7] as expressed in eqs (10) and (11), was further verified in this work, and can now be simply established for any material and gage geometry. The applicability of the quasi-static procedure to the dynamic case is verified in Part II of this work. The k_i coefficients are related to some extent to the actual plastic modulus. The degree of influence is related to the plastic modulus itself, mostly for k_2 and k_3. However, it was found that these coefficients are almost unaffected by the material properties and gage width, when the latter is wider (Table 3). Therefore, for a given material, the best accuracy is expected when testing "large" gage specimens (e.g. $w = 2$ mm). The average strain is dictated by k_3, so that prior knowledge on the anticipated plastic properties will be useful in planning the experiments for an anticipated strain. Keeping in mind the above-mentioned, this relationship is of huge practical interest, and is the first of its kind for such a shear specimen.

Finally, the present work confirms that the SCS geometry can confidently be used for the characterization of large strain behavior of materials. As such, the present results are among the most thorough analyses presented for new specimens of that kind.

Conclusions

The SCS has been thoroughly analyzed numerically for quasi-static loading conditions. Bi-linear material behavior has been assumed, as a first step for the present analysis. Specific issues that were not addressed previously have been investigated, and the following conclusions can be drawn from the present work.

- The stresses and strains are quite homogeneous in the gage section.
- Stress concentration at the gage fillets indeed exists but is of minor influence on the determined mechanical properties.
- Very simple relations have been developed to reduce the load–displacement curve into an equivalent stress–strain relationship in terms of three coefficients. These coefficients are material- and gage-geometry-dependent, and guidelines have been provided for their determination.

- Additional work should be carried out to include other types of material behavior, such as parabolic.

Acknowledgments

Support of the Lady Davis Postdoctoral Fund at Technion to AD is acknowledged. DR acknowledges the partial support of the Fund for Promotion of Research at Technion (grant 030-168). Useful discussions with G. Ravichandran and M. Vural are gratefully acknowledged.

References

1. Green, D.E., Neale, K.W., MacEwen, S.R., Makinde, A., and Perrin, R., "Experimental Investigation of the Biaxial Behavior of an Aluminum Sheet," International Journal of Plasticity, **20** *(8–9), 1677–1706 (2004).*

2. Arcan, M., Hashin, Z., and Voloshin, A.S., "A Method to Produce Uniform Plane-Stress States with Applications to Fiber-reinforced Materials," EXPERIMENTAL MECHANICS, **l8** *(4), l4l–l46 (l978).*

3. Khan, A.S. and Wang, X., "An Experimental Study of Finite Plastic Deformation in Annealed 1100 Aluminum During Proportional and Non-proportional Biaxial Compression," International Journal of Plasticity, **6** *(4), 485–504(1990).*

4. Wang, X.F. and Lee, L.H.N., "Post-bifurcation Behavior of Wrinkles in square Metal Sheets under Yoshida Test," International Journal of Plasticity, **9** *(1), 1–19 (1993).*

5. Nouailhas, D. and Cailletaud, G., "Tension–torsion Behavior of Single-crystal Superalloys—Experiment and Finite-element Analysis," International Journal of Plasticity, **11** *(4), 451–470 (1995).*

6. Roessig, K.M. and Mason, J.J., "Adiabatic Shear Localization in the Dynamic Punch Test. Part II: Numerical Simulations," International Journal of Plasticity, **15** *(3), 263–283 (1999).*

7. Rittel, D., Ravichandran, G., and Lee, S., "A Shear Compression Specimen for Large Strain Testing," EXPERIMENTAL MECHANICS, **42** *(1), 58–64 (2002).*

8. Rittel, D., Ravichandran, G., and Lee, S., "Large Strain Constitutive Behavior of OFHC Copper over a Wide Range of Strain Rates Using the Shear Compression Specimen," Mechanics of Materials, **34** *(10), 627–642 (2002).*

9. Vural, M., Rittel, D., and Ravichandran, G., "Large Strain Mechanical Behavior of 1018 Cold Rolled Steel over a Wide Range of Strain Rates," Metallurgical and Material Transactions A, **34A** *(12), 2873–2885 (2003).*